Cohesive Fracture Analysis to Model Multiple-Stage Fracturing in Quasibrittle Shale Formations

M. Haddad and K. Sepehrnoori

The University of Texas at Austin (TX, USA), Petroleum and Geosystems Engineering Department

Abstract*: Over the last three decades, shale gas reservoirs have emerged as gigantic gas resources. Economic production from shale gas cannot be achieved by natural mechanisms alone; it requires technologies such as hydraulic fracturing in multiple stages along a horizontal wellbore. Developing numerical models for hydraulic fracturing is essential since a successful fracturing job in a shale formation cannot be generalized to another due to different shale characteristics, and restricted access to the field data acquisition. Empirical methods and Linear Elastic Fracture Mechanics (LEFM)-based numerical techniques are still the prevailing design tools in most hydraulic fracture applications though they provide a reasonable prediction only for hard (brittle) rocks. The plastic zone and softening effects at the fracture tip have been neglected in modeling hydraulic fracturing, which results in the prediction of conservative fracture geometry and imprecise fracture pressure. These effects can be identified by the Cohesive Zone Model (CZM) but not by LEFM. Moreover, CZM is able to model fracturing interfaces; for instance, natural fractures, which are mechanically weaker than the adjoining materials. In addition, petrophysical log data has extended the range of ductility in shale layers even though these layers belong to the same shale formation. Brittle shales are more likely to contain more natural fractures while ductile shales act as good seals for the fractured layers. In this work, we modeled multiple-stage fracturing in a quasibrittle shale layer using an improved CZM for porous media besides including the material softening effect. We sought to determine the superiority of CZM compared to LEFM in shales. Also, we investigated various scenarios in number and sequence of fracturing stages for different rock properties. Moreover, we examined the fracture behavior after the fracturing fluid shut-in. We found that the stress shadow effects on induced fractures significantly influenced the characteristics of subsequent induced fractures.*

Keywords*: Hydraulic fracture, Pore pressure, Cohesive zone model, Ductile and brittle rocks, Finite Element Method, Stress shadow effects.*

1. Introduction

Shale gas resources are organic-rich formations which can provide a long-lasting source of gas. These reservoirs will move the U.S. from a natural gas importer to an exporter by 2019 (EIA, 2013). Crucial to enhancing gas flow in the shale reservoirs are natural fractures since they behave like flow channels connecting the non-producing zones of gas to the wellbore. However, economic production from shale gas cannot be achieved by natural mechanisms alone; it requires technologies like horizontal drilling and hydraulic fracturing, the most common methods of production stimulation in shale gas reservoirs.

The obstacles of data acquisition from fracturing jobs, and generalizing the data from one successful fracturing job to another (Rickman et al., 2008) necessitate developing analytical or numerical optimizing tools for hydraulic fracturing. The simulation of hydraulic fracturing is a multi-physics problem that couples fluid mechanics with solid and fracture mechanics; the driving force of fracturing is the fluid pressure on the fracture walls. Fluid leak-off depends on fracturing fluid pressure and more leak-off causes more pressure drop along a fracture and less fracture propagation. Natural fractures and pre-existing hydraulic fractures can deviate the consecutively induced fractures, which is known as the stress shadowing effect.

The first attempts at mathematical simulation of hydraulic fracturing dates back to the 1960s when Perkins and Kern (1961) offered simplifying assumptions for an extremely complex problem which included simplified fluid flow, fracture shape and leakage from the fracture. This attempt was followed by restricted analytical solutions mostly in the context of Linear Elastic Fracture Mechanics (LEFM) for stationary simple cracks, Rice and Cleary (1976) and Cleary (1978). The development of these analytical models led to the three most well-known 2D models, PKN (Nordgren, 1972), KGD (Daneshy, 1973), and penny-shaped fracture (Abe et al., 1976). Fractures in these models are bi-wing with assumed shapes. Subsequently, a pseudo 3D model (P3DH) was proposed by Settari and Cleary (1986) in which a single vertical fracture can propagate in both lateral and vertical directions in the fracture plane. In this 3D model, the fracture opening is obtained by solving a boundary integral equation. However, it is strongly sensitive to confining stress, stiffness contrast of adjacent strata, and fluid properties. Also, because the model neglects the vertical fluid flow component, it over-predicts fracture height for a poorly contained fracture. Subsequently, a model for a 2D solution-dependent moving crack including fluid leakage was proposed by Boone and Ingraffea (1990) and modified by Carter et al. (2000) for a fully 3D hydraulic fracture, but that model neglected fluid continuity in the medium surrounding the fracture.

The boundary integral or displacement discontinuity method has been widely adopted for crack modeling. This method was proposed for the first time by Crouch (1976) and Crouch et al. (1983) to evaluate the mixed mode stress intensity factors and crack propagation simulation using a quadratic scheme to enhance the solution accuracy for curved cracks. Recently, Wong et al. (2013) modeled non-planar 3D fracture growth in linear elastic medium using boundary integral equations and LEFM-based fracture propagation criteria applied selectively on a group of virtual elements. Their model took into account the viscosity and toughness controlled fracture growth as well as fluid lag behavior, fluid loss using Carter's leak-off model, and heterogeneous in-situ stress. The displacement discontinuity technique results in efficient and accurate fracture propagation in elastic homogeneous media. However, the main advantage of the boundary integral method, discretising just the boundary of the body, can become a serious challenge in problems with unknown boundaries, such as crack propagation, which need re-meshing and can lead to simulation difficulties (Huang et al., 2012). Also, this method has limited applicability for heterogeneous reservoirs (Lecampion, 2009).

Empirical methods and LEFM-based boundary integral (displacement discontinuity) techniques are still the prevailing design tools in most hydraulic fracture applications while they provide a reasonable prediction for hard (brittle) rocks. These methods predict conservatively if applied to ductile or quasi-brittle shale and other soft rocks such as clay or weakly consolidated sandstones because they neglect the fracture process zone ahead of the crack tip (Yao, 2011). A cohesive fracture mechanics-based method can include the fracture tip effects such as material softening in quasi-brittle rocks such as shales.

The cohesive method can be adopted using the Finite Element Method (FEM) to investigate multiple-stage fracturing in heterogeneous resources. Here, heterogeneity can include in-situ stress, elastic modulus, Poisson's ratio, fracture toughness, pore pressure, and leak-off coefficients.

This work focuses on the stress interaction of hydraulic fractures propagating under different injection scenarios. The hydraulic fractures are modeled using cohesive elements in the FEM framework. Depending on the fracture spacing, each propagating fracture can be influenced by the stress shadows of the other pre-existing or propagating fractures. The influenced characteristics include fracture aperture and length.

The results of this work introduce a rigorous model that uses the cohesive fracture mechanics-based method to optimize multiple-stage hydraulic fracturing jobs especially in pseudo-brittle shale resources. Shale resources typically include numerous natural fractures which influence the propagation of hydraulic fractures. This influence is one of the targets of the current work. Also, significant production enhancement due to complex fracture networks in shale formations motivates the operators to proliferate the number of fracturing stages and fractures per stage; this promotes the interaction of hydraulic fractures, which requires a practical tool to model that interaction.

This work contains the following sections: description of the mathematical model for cohesive fracture analysis, CZM; simulation results; and conclusions. Parametric studies allow us to determine the most important parameters in fracture propagation under stress shadowing effects of pre-existing fractures.

2. Method

The concept of cohesive zones was applied to fracture modeling for the first time after the works done by Dugdale (1960) and Barenblatt (1962). Needleman (1987) argued that cohesive elements are attractive when interface strengths are relatively weak compared to the adjoining materials; for instance, the strength of cement in a natural fracture is weaker than the surrounding rock strength. Cohesive behavior models the separation between two initially bonded surfaces. This model idealizes complex fracture mechanisms using a macroscopic "cohesive law", which is the relation between the traction across the interface and the separation and includes damage initiation and evolution conditions, necessary for progressive damage. Figure 1 demonstrates the traction-separation response for a specific mode mix combination.

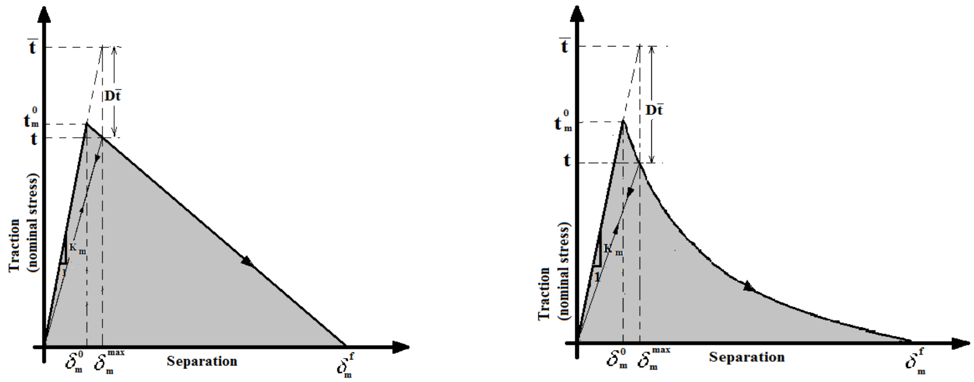

Figure 1. Typical cohesive traction separation law;

linear damage evolution (left), and exponential damage evolution (right).

t_m^0 and δ_m^0 in Figure 1 are respectively the size of mixed-mode traction stress and separation vectors at damage initiation. The corresponding stress and separation vectors are governed by the following elastic constitutive law:

$$\vec{t} = \begin{Bmatrix} t_n \\ t_s \\ t_t \end{Bmatrix} = \begin{bmatrix} K_{nn} & K_{ns} & K_{nt} \\ K_{ns} & K_{ss} & K_{st} \\ K_{nt} & K_{st} & K_{tt} \end{bmatrix} \begin{Bmatrix} \varepsilon_n \\ \varepsilon_s \\ \varepsilon_t \end{Bmatrix} = \left(\frac{1}{T_0}\right) \vec{\vec{K}}.\vec{\delta}, \tag{1}$$

where $\vec{t}$ is the traction stress vector on the cohesive zone interface, $\vec{\delta}$ denotes the interface separation, and T_0 is the cohesive zone initial thickness. The off-diagonal terms in the elasticity matrix vanish for the uncoupled behavior between the normal and shear components. Moreover, damage in a traction-separation response is quantified by the deviation from the elastic material behavior as below:

$$t_n = \begin{cases} (1-D)\bar{t}_n, \ \bar{t}_n \geq 0 \\ \bar{t}_n, \ otherwise \ (no\ damage\ to\ copressive\ stiffness) \end{cases}, \tag{2}$$

$$t_s = (1-D)\bar{t}_s, \tag{3}$$

$$t_t = (1-D)\bar{t}_t, \tag{4}$$

where $\bar{t}_n$, $\bar{t}_s$, and $\bar{t}_t$ are the stress components predicted by the elastic traction-separation behavior for the current strains without damage. Here, D is known as the damage variable and is evaluated by the post-elastic traction-separation response. The cohesive elements with zero load carrying capacity, D=1, at all integration points compose the fully degraded (failed) elements or the induced fracture; the fracture tip is located where partially and fully degraded cohesive elements reach each other.

Progressive damage is accomplished by two essential consecutive steps: 1) damage initiation, and 2) damage evolution. Among various damage initiation and evolution criteria, the common ones are the quadratic nominal stress and BK model, respectively. These criteria integrate all probable mixed-mode damage mechanisms simultaneously. The damage variable, D, in energy-based evolution is specified by either a linear (default) or exponential softening response.

The Cohesive Zone Model (CZM) must be modified to become applicable for modeling hydraulic rock failure as a result of fluid pressure in the fracture gap. In this model, fracturing is a gradual material damage process in which separation of fracture walls is resisted by cohesive traction which now includes the cohesive zone pore pressure. This model, known as the pore pressure cohesive zone model, has been adopted in the finite element program Abaqus, and includes the most important features of hydraulic fracturing, crack propagation and fracture fluid flow.

Cohesive elements potentially cause nonlinear and non-smooth structural responses leading to numerical difficulties in solution convergence. Moreover, in implicit analysis programs such as Abaqus/Standard, unstable crack propagation through cohesive elements often causes convergence problems. This problem is resolved in Abaqus using built-in viscous regularization which permits stresses to be outside the limits set by the traction-separation law and is defined by Equation 5 (Abaqus Analysis User's Manual).

$$\dot{D}_v = \frac{1}{\mu}\left(D - D_v\right), \tag{5}$$

where μ is the viscosity relaxation parameter and D is the damage variable calculated in the inviscid backbone model. Therefore, the damaged viscous material shows the following response:

$$t = \left(1 - D_v\right)\bar{t}. \tag{6}$$

A small value for the viscosity parameter with respect to characteristic time increment usually improves the rate of convergence in the softening regime; it has a minimal effect on the solution. Ideally, the solution of the viscous system relaxes to that of the inviscid case as $t/\mu \to \infty$, where t denotes time.

A hydraulic fracture flow model should consist of two components: 1) fluid leak-off, a prevalent characteristic of induced fractures, and 2) tangential flow through the fracture. The first component influences two patterns: 1) the fracture propagation, and 2) proppant placement. The latter pattern depends on fracturing pad leak-off into the formation in order to let the proppant slug move forward. Generally, leak-off is assumed uncoupled from the fluid pressure and restricted to linear, 1D flow regimes mainly based on Carter's 1D fluid flow model (Howard and Fast, 1957). The pore pressure cohesive zone model in Abaqus provides both hydraulic fracture flow components in a rigorous continuum- or Darcy-based approach; it constructs the leak-off component by the filter cake permeability times the pore pressure gradient perpendicular to fracture walls and the tangential flow component by the Reynolds' permeability times the pore pressure gradient along fractures.

In order to incorporate a cohesive zone model into the finite element model, the principle of virtual work is extended to represent stress equilibrium for the consolidating solid phase under fracture wall tractions in the current configuration at time *t*:

$$\int_V \left(\vec{\vec{\bar{\sigma}}} - \chi u_w \vec{\vec{I}} \right) : \delta\vec{\vec{\varepsilon}} dV = \int_S \vec{t} . \delta\vec{v} dS + \int_V \vec{f} . \delta\vec{v} dV + \int_V sn\rho_w \vec{g} . \delta\vec{v} dV, \tag{7}$$

where $\vec{\vec{\bar{\sigma}}}$ is effective stress tensor defined as Equation 8, $\delta\vec{\vec{\varepsilon}}$ is the virtual deformation rate tensor, $\vec{t}$ is surface tractions vector per unit area, $\delta\vec{v}$ is a virtual velocity field vector, $\vec{f}$ is body forces vector (excluding fluid weight) per unit volume, ρ_w is the density of the fluid, and $\vec{g}$ is the gravitational acceleration vector. Also, *S* and *V* represent integration on fracture surface and bulk volume, respectively. The effective stress for saturated porous media is defined as

$$\vec{\vec{\bar{\sigma}}} = \vec{\vec{\sigma}} + u_w \vec{\vec{I}}, \tag{8}$$

where $\vec{\vec{\sigma}}$ is total stress tensor, u_w is the wetting phase pressure, and $\vec{\vec{I}}$ is the identity matrix.

Equation 7 is discretized using a Lagrangian formulation for the porous media, with displacements and pore pressures as the nodal variables. The porous medium is modeled by attaching the finite element mesh to the solid phase. Fluid can flow through this mesh, which is governed by a continuity equation as

$$\frac{d}{dt}\left(\int_V \frac{\rho_w}{\rho_w^0} sndV \right) = -\int_S \frac{\rho_w}{\rho_w^0} sn\vec{n}.\vec{v}_w dS, \tag{9}$$

Where ρ_w^0 is the reference density of the fluid, and $\vec{n}$ is the outward normal to *S*. v_w is the average velocity of the fluid relative to the solid phase (the seepage velocity) and is defined according to Darcy's or Forchheimer's law.

The fully coupled solution of fluid continuity and stress equilibrium is the big advantage of modeling porous media in Abaqus. The transient problem requires time integration of the diffusion effects. Therefore, the time increment should be selected carefully. The integration procedure in Abaqus/Standard for consolidation analysis requires a minimum usable time increment depending on the element size; for instance, for a saturated flow problem as in the following:

$$\Delta t > \frac{\gamma_w}{6Ek} \left(\Delta \ell \right)^2, \tag{10}$$

where γ_w is the specific weight of the wetting liquid, *E* is Young's Modulus, *k* is the permeability of the soil, and $\Delta\ell$ is a typical element dimension. If smaller time increments than the minimum are used, spurious oscillations may happen. In order to use smaller time increments, the mesh should be refined. The upper limit on time increment size is dependent on accuracy, not on the solution stability and the integration procedure is unconditionally stable except for the possible numerical problems due to the nonlinearities.

Hydraulic fracturing is coincident with large deformations; it requires a finite-strain (in contrast to infinitesimal-strain) consolidation analysis. For instance, finite-strain analysis results in around 40% more deformations than that in small strain analysis in the Terzaghi consolidation problem

(Abaqus Analysis User’s Manual). In contrast to small strain analysis, finite strain analysis causes significant changes in element volumes and consequently, to element porosity and permeability.

Most geotechnical problems have initial nonzero stress states in the medium. The response of a system differs for various initial stress states, specifically in nonlinear analyses. Abaqus provides the geostatic procedure to set up the initial stress state. The initial effective stresses due to the geostatic loading can be specified as model data. However, it may be difficult to specify initially equilibrated stresses with the geostatic loads. The geostatic procedure re-establishes the initial equilibrium based on specified boundary conditions and external field loads such as gravity. However, in some problems, the geostatic procedure is inadequate and it is crucial to specify the correct initial conditions; otherwise, the system is initially out of equilibrium which might lead to failure in starting the solution. For instance, saturated flow analyses require consistent total and effective stress values on boundaries depending on their depth, grain and wetting phase specific weight, saturation, and porosity.

3. Results and Discussion

One of the advantages of our 3D fracturing model is its capability to simulate propagating multiple-stage fractures. Therefore, we are able to investigate different configurations for multiple stage fractures. In the first case, to demonstrate the interaction of multiple fractures while propagating, we built two simple hydraulic fracturing models in Abaqus for single- and double-stage fracturing as shown in Figures 2 and 3, respectively. The ultra-thin cohesive elements can be indirectly identified by the finer grids around them. These models are plane strain fully coupled pore pressure/stress analysis models for single phase flow in a homogeneous reservoir containing two straight planes on which the cohesive fractures propagate according to the quadratic stress criterion for fracture initiation, and an energy-based mix-mode BK model for fracture evolution. Gap flow is Newtonian with a specified viscosity. Table 1 summarizes the required information to construct these single- or double-stage fracture models.

Table 1. Summary of the input data for the 2D plane strain hydraulic fracturing model; the first case

Model	Setting		Parameter	Single layer: Target
Cohesive layer properties, Element type: COH2D4P	**Elastic Type: Traction**		$K_{nn} = K_{ss}\ (kPa)$	8.5×10^{7}
	Damage Initiation Criterion: Quads		$N_{\max}, S_{\max}\ (kPa)$	320, 1.0×10^{10}
	Damage Evolution Type: Energy, BK Mixed Mode ($\eta = 2.284$)		$G_{Ic} = G_{IIc}\ (N/mm)$	28
	Gap flow (water)		Dynamic Viscosity (kPa.s)	1.0×10^{-6}
			Leak-off coefficient ($m^3/kPa.s$)	5.879×10^{-10}
Porous material properties, Element Type: CPE4RP	**Elastic model**		Young's modulus (kPa)	1.294×10^{6}
			Poisson's ratio	0.25
	Permeability, specific density= ρg_w **= 9.8 kPa/m**		Permeability (m/s)	2.418×10^{-8}
Model Setup	**Shape**	**Reservoir: a cartezian 2D oil reservoir, Half by symmetry**	Elevation (m) x Length (m)	$-(2000\ to\ 1880)\times 240$
		Fracture: two vertical planar surfaces	Height (m) x Initial thickness (m)	$Right: 40\times0.001325\ starting\ at\ (40,-2000)$ $Left: 40\times0.001325\ starting\ at\ (-40,-2000)$
	Initial conditions		Initial void ratio	0.333333
			Initial pore pressure (kPa)	793
			Initial effective stress (kPa)	0
			Initial oil saturation	100%
	Boundary conditions		Y- fixing	On the horizontal lower wall
			X- and Y- fixing	On the other walls
	Steps (the third step is applicable for double-stage fracturing)		Soils consolidation, transient nonlinear analysis for 700 sec	Hydraulic fracturing step
			Soils consolidation, SS nonlinear analysis for 7200 sec	To reach steady state condition after fracturing
			Soils consolidation, transient nonlinear analysis for 700 sec	Hydraulic fracturing step
	Fracturing fluid injection		Volume flow rate ramp (m^3/s)	0 sec, 0, 63 sec, -0.001 in 1 element

Figure 4 compares final fracturing fluid pressure along the propped fracture for single- and double-stage fracturing cases. Figure 5 shows the fracturing fluid pressure history in these two cases. Both Figures 4 and 5 show that simultaneous fracturing in two stages needs 2000 kPa higher fracturing fluid pressure than in one stage.

Figure 6 compares fracture width development over time for single- and double-stage fracturing. This figure shows that single stage fracturing leads to longer and narrower fractures whereas double-stage fracturing results in shorter and wider fractures. This is due to the stress shadowing effect of a pre-existing propped fracture on the new emerging fracture as this effect prevents fractures from propagating in length while the conservation of mass induces a wider fracture.

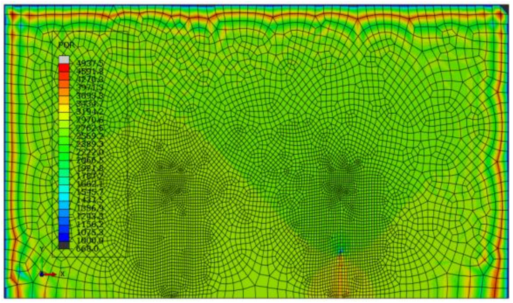

Figure 2. Pore pressure distribution at the end of single-stage hydraulic fracturing.

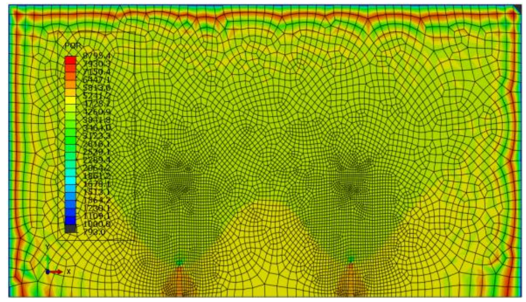

Figure 3. Pore pressure distribution at the end of simultaneous double-stage hydraulic fracturing.

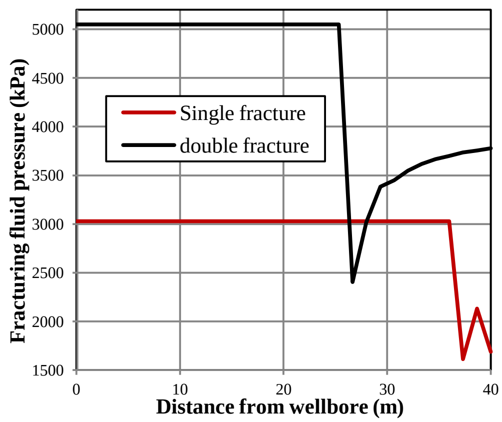

Figure 4. Comparison of final fracturing fluid pressure along the fracture(s) in single or double stage fracturing cases.

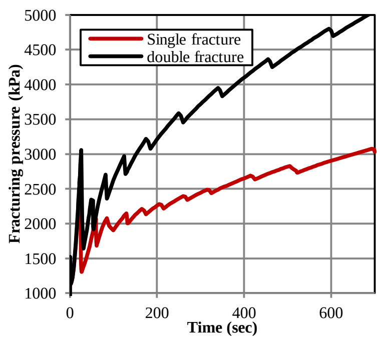

Figure 5. Comparison of fracturing fluid injection pressure for single- and simultaneous double-stage hydraulic fracturing cases.

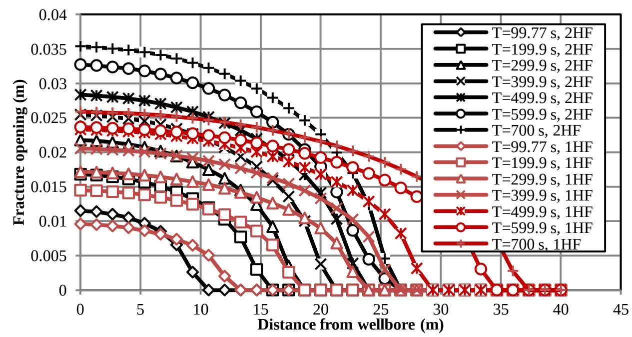

Figure 6. Comparison of fracture opening along the right fracture for single- and simultaneous double-stage hydraulic fracturing cases.

In the second case, we investigated the fracture behavior after shut-in. In this case, fracturing fluid was injected for a shorter period of time (1/7 of that in the previous case) with a higher flow rate (8 times more) compared to the first case. Figures 7 and 8 demonstrate injection pressure and the fracture opening, respectively, during the whole process for single- and double-stage fracture(s). After shut-in, fracture(s) is (are) still growing. This growth is more significant in the model for double fractures (~72%) compared to the model for a single fracture (~40%). Also, it takes longer for the double-stage fractures (666.5 seconds) compared to the single-stage one (490.5 seconds) to reach a steady state fracture length.

Fracture growth after shut-in possibly originates from fixed solid boundary conditions, and unsteady stress state. Moreover, at the end of injection, the fluid flow was suddenly stopped in the fracture entrance such that during shut-in, fracturing fluid is not able to flow back to the wellbore. Also, because low-permeable media leads to low leak-off into the formation, the injected fluid is trapped in the fracture space, which causes a non-equilibrium stress state in the formation. This fracture closure pushes the trapped fluid toward the fracture tip, which leads to more fracture propagation.

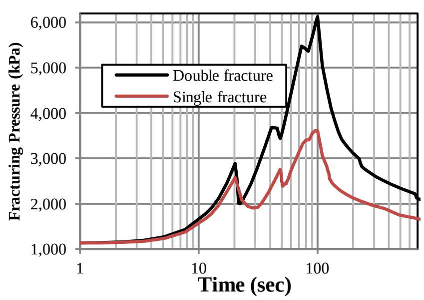

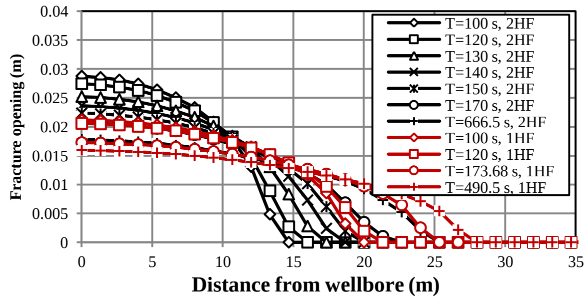

Figure 7. Comparison of injection pressure for single- and simultaneous double-stage hydraulic fracturing cases including shut-in.

Figure 8. Comparison of fracture opening along right fracture for single- and simultaneous double-stage hydraulic fracturing cases while shut-in.

In the third case, we investigate the effects of pre-existing hydraulic fractures on the current propagating fracture. Compared to the second case with simultaneous fracturing, in this problem, fracturing fluid is injected in the right and left perforation locations, consecutively. Figures 9 and 10 show the contours for stress component S11 at the beginning and at the end of the second-stage fracturing, respectively. These figures show the stress shadow due to the right hydraulic fracture, and its effect on the second stage fracturing, respectively. Figure 10 demonstrates that due to the stress shadowing effect, the second stage fracture is shorter and wider than the first one. Moreover, in another result not shown here, the contour for shear stress sheds light on the contribution of the shear stress component to the reluctance of the second-stage fracture to propagate lengthwise. Due to mode-mixity, some part of total fracture energy is consumed by the shear deformations instead of opening displacements, which causes shorter fractures.

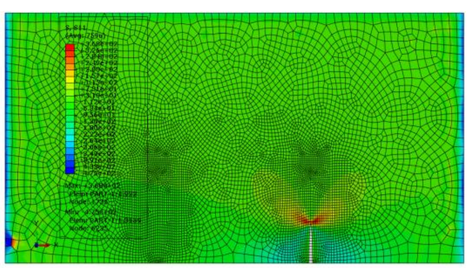

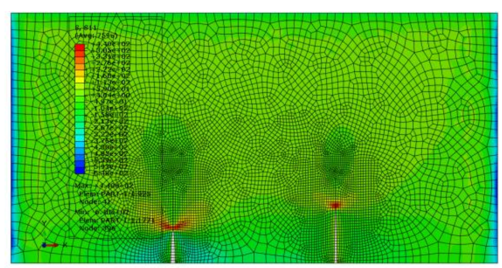

Figure 9. Residual stress component S11 at the beginning of the second stage fracturing for consecutive double-stage fracturing.

Figure 10. Final stress component S11 for consecutive double-stage fracturing, a shorter second fracture than the first one.

Figure 11 compares the fracture widths in the consecutive and simultaneous double-stage fracturing, the second and third cases, respectively. Fracturing fluid injection is done for 100 seconds for each fracture followed by a steady state step in both cases. In the consecutive case, at the end of injection (100 seconds per fracture), the left fracture is wider compared to the right one whereas the fracture length has the opposite trend. Also, Figure 12 shows the temporal and spatial change of fracture openings for the right and left fractures, which do not follow the same trend. These two figures demonstrate the stress shadowing effect of the opened right fracture on the left one.

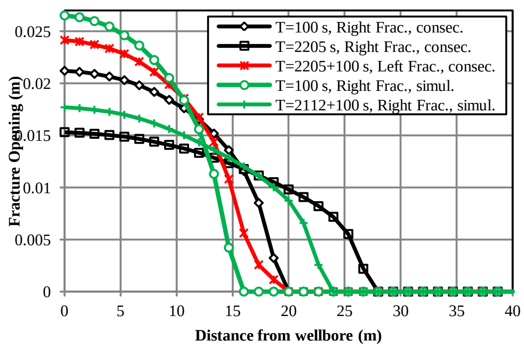

Figure 11. Comparison of fracture width at the end of analysis steps for consecutive and simultaneous fracturing.

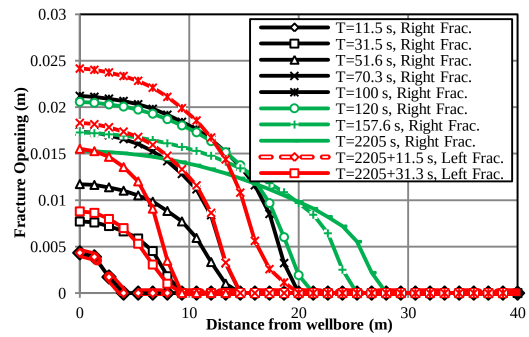

Figure 12. Temporal variation of fracture width for consecutive double-stage hydraulic fracturing.

Figure 13 consists of two sub-figures: 1) upper figure, the injection and pore pressure in the right and left fracturing stages, respectively, and 2) lower figure, the injection and pore pressure in the left and right fracturing stages, respectively. While fracturing the right or left stage, pore pressure at the left or right stage increases smoothly; this demonstrates the stress shadowing effect of each fracture on the other since the opening fracture exerts a confining stress on the media surrounding the fracture.

Figure 14 compares the contribution in total energy of the damage and viscous regularization energy dissipation. Viscous regularization stabilizes the numerical analysis and its desirable minimal effect on the solution can be examined by its associated energy dissipation out of the total energy. During the first or second stage fracturing, viscous regularization contributes 25% of the total energy. Damage dissipation energy has almost the same trend. The contribution of viscous regularization energy dissipation of total energy may be reduced by optimizing the associated viscosity parameter; however, this optimization has not been studied here and is recommended for future works.

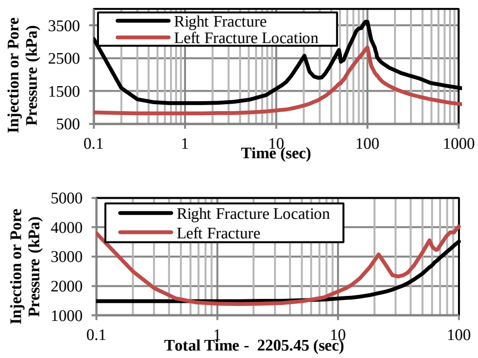

Figure 13. Injection and pore pressure in the right and left fractures or locations for consecutive hydraulic fracturing.

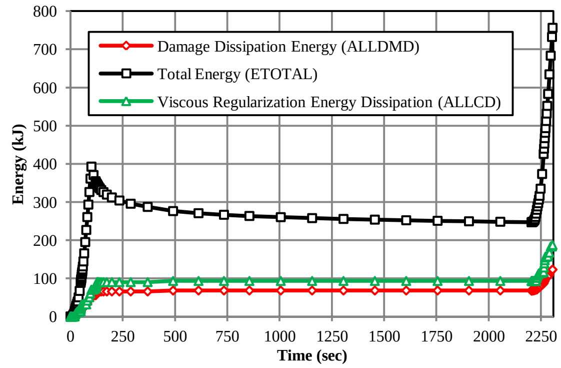

Figure 14. Comparison of total, damage dissipation, and viscous regularization energies for the consecutive hydraulic fracturing case.

4. Conclusions

In this paper, using a fully coupled pore pressure-stress analysis, we solved two dimensional single- and double-stage hydraulic fracturing problems. The fractures were modeled using a pore pressure cohesive zone model, an advantageous model with respect to LEFM for quasibrittle rocks such as shales due to a more rigorous treatment with the process zones ahead of the fracture tips. The fully coupled analysis provided us with a continuum-based leak-off model eliminating the requirement for an explicit leak-off model such as Carter's leak-off model. Production from ultra-low permeable shale gas resources requires closely spaced hydraulic fractures which have mechanical interactions or stress shadowing effects with each other. We proved the benefits of modeling multiple-stage fractures using our numerical method, FEM, demonstrating the stress shadowing effect of pre-existing or simultaneously growing fractures on the other fractures. This effect was observed in the following: (1) shorter and wider fractures in the simultaneous fracturing case compared to the single stage fracturing case, (2) fracture closure due to residual stresses in the media, (3) a shorter and wider fracture due to a pre-existing fracture in the consecutive fracturing case, and (4) the excitement of the mixed-mode fracture growth in the second stage of fracturing due to the residual stresses of the first-stage fracturing.

5. Acknowledgment

This work was sponsored by the Center for Petroleum and Geosystems Engineering at The University of Texas at Austin.

6. References

1. Abaqus Analysis User's Manual, Version 6.12, Dassault Systémes Simulia Corp., Providence, RI.
2. Abe, H., Keer, L.M., and Mura, T., "Growth rate of a penny-shaped crack in hydraulic fracturing of rocks", Journal of Geophysical Research, 81(35), 6292-6298, 1976.
3. Barenblatt, G., "The mathematical theory of equilibrium cracks in brittle fracture", Advances in Applied Mechanics, 7, 55-129, 1962.
4. Boone, T.J., and Ingraffea, A.R., "A numerical procedure for simulation of hydraulically driven fracture propagation in poroelastic media", Int J Numer Anal Methods Geomech., 14, 27–47, 1990.
5. Carter, B.J., Desroches, J., Ingraffea, A.R., and Wawrzynek, P.A., "Simulating fully 3-D hydraulic fracturing. In: Zaman, Booker and Gioda (eds) Modeling in geomechanics", Chichester, England, Wiley, 525–567, 2000.
6. Cleary M.P., "Moving singularities in elasto-diffusive solids with applications to fracture propagation", Int J Solids Struct., 14, 81-97, 1978.
7. Crouch, S.L., "Solution of plane elasticity problems by the displacement discontinuity method", Int. J. Numer. Methods Engrg., 10, 301-343, 1976.
8. Crouch, S.L., and Starfield, A.M., "Boundary element methods in solid mechanics", London, England, Allen & Unwin, 1983.
9. Daneshy, A.A., "On the design of vertical hydraulic fractures", Journal of Petroleum Technology, 25(1), 83-97, 1973.
10. Dugdale, D., "Yielding of steel sheets containing slits", Journal of the Mechanics and Physics of Solids, 8, 100-104, 1960.
11. "EIA 2013", Annual Energy Outlook, The U.S. Energy Information Administration, 2013.
12. Huang, K., Zhang, Z., and Ghassemi, A., "Modeling three-dimensional hydraulic fracture propagation using virtual multidimensional internal bonds", Int. J. Numer. Anal. Meth. Geomech, 2012.
13. Lecampion, B., "An extended finite element method for hydraulic fracture problems", Commun. Numer. Meth. Engng, 25, 121-133, 2009.
14. Needleman, A., "A continuum model for void nucleation by inclusion debonding", Journal of applied mechanics, 54(3), 525-531, 1987.
15. Nordgren, R.P., "Propagation of a vertical hydraulic fracture", SPE Journal, 12(4), 306-314, 1972.
16. Perkins, T.K., and Kern, L.R., "Widths of hydraulic fractures", SPE Journal of Petroleum Technology, 13(9), 937-949, 1961.
17. Rice, J.R., and Cleary, M.P., "Some basic stress diffusion solutions for fluid saturated elastic porous media with compressible constituents", Rev Geophys Space Phys, 14, 227–241, 1976.
18. Rickman, R., Mullen, M., Petre, E., Grieser, B., and Kundert, D., "A practical Use of Shale Petrophysics for stimulation design optimization: All shale plays are not clones of the Barnett shale", Paper SPE presented at the 2008 SPE Annual Technical Conference and Exhibition, Denver, Colorado, USA, 21-24 September, 2008.

19. Settari, A. and Cleary, M.P., "Development and testing of a pseudo three-dimensional model of hydraulic fracture geometry", SPE Production Engineering Journal, 1(6), 449-466, 1986.
20. Howard, G.C. and Fast, C.R., "Optimum fluid characteristics for fracture extension", Presented by G.C. Howard at the spring meeting of the Mid-Continent District, Division of Production, Tulsa, Oklahoma, USA, April, 1957.
21. Wong, S., Geilikman, M., and Xu, G., "The Geomechanical Interaction of Multiple Hydraulic Fractures in Horizontal Wells", Effective and Sustainable Hydraulic Fracturing (ed. R. Jeffrey), Available from http://dx.doi.org/10.5772/56385, 2013.
22. Yao, Y., "Linear Elastic and Cohesive Fracture Analysis to Model Hydraulic Fracture in Brittle and Ductile Rocks", Rock Mech Rock Eng, DOI 10.1007/s00603-011-0211-0, 2011.